

Electronic Supplementary Information

GaAs Nanoscale Membranes: Prospects for Seamless Integration of III-Vs on Silicon

Andrés M. Raya,^{ab‡} Martin Friedl,^{a‡} Sara Martí-Sánchez,^{c‡} Vladimir G. Dubrovskii,^d Luca Francaviglia,^a Benito Alén,^b Nicholas Morgan,^a Gözde Tütüncüoğlu,^a Quentin M. Ramasse,^{ef} David Fuster,^b Jose M. Llorens,^b Jordi Arbiol,^{cg} and Anna Fontcuberta i Morral^{ah*}

^a Laboratoire des Matériaux Semiconducteurs, Institute of Materials, Faculty of Engineering, École Polytechnique Fédérale de Lausanne, EPFL, 1015 Lausanne, Switzerland

^b Instituto de Micro y Nanotecnología, IMN-CNM, CSIC (CEI UAM+CSIC), Isaac Newton, 8, 28760 Tres Cantos, Madrid, Spain

^c Catalan Institute of Nanoscience and Nanotechnology (ICN2), CSIC and BIST, Campus UAB, Bellaterra, 08193 Barcelona, Catalonia, Spain

^d ITMO University, Kronverkskiy pr. 49, 197101 St. Petersburg, Russia

^e SuperSTEM Laboratory, SciTech Daresbury Campus, Daresbury WA4 4AD, United Kingdom

^f School of Chemical and Process Engineering, and School of Physics, University of Leeds, Leeds LS2 9JT, United Kingdom

^g ICREA, Pg. Lluís Companys 23, 08010 Barcelona, Catalonia, Spain

^h Institute of Physics, Faculty of Basic Sciences, École Polytechnique Fédérale de Lausanne, EPFL, 1015 Lausanne, Switzerland

[‡]Equal contribution

*E-mail: anna.fontcuberta-morral@epfl.ch

1 EELS maps showing material diffusing on top of GaAs cap of passivated NMs

Electron energy loss spectroscopy (EELS) spectrum images were acquired in a TECNAI F20 microscope operated at 200 kV with an energy resolution of 2 eV (FWHM). Signal integration was performed after power law background extraction using Ga $L_{3,2}$, As $L_{3,2}$, Al K and Si K major edges.

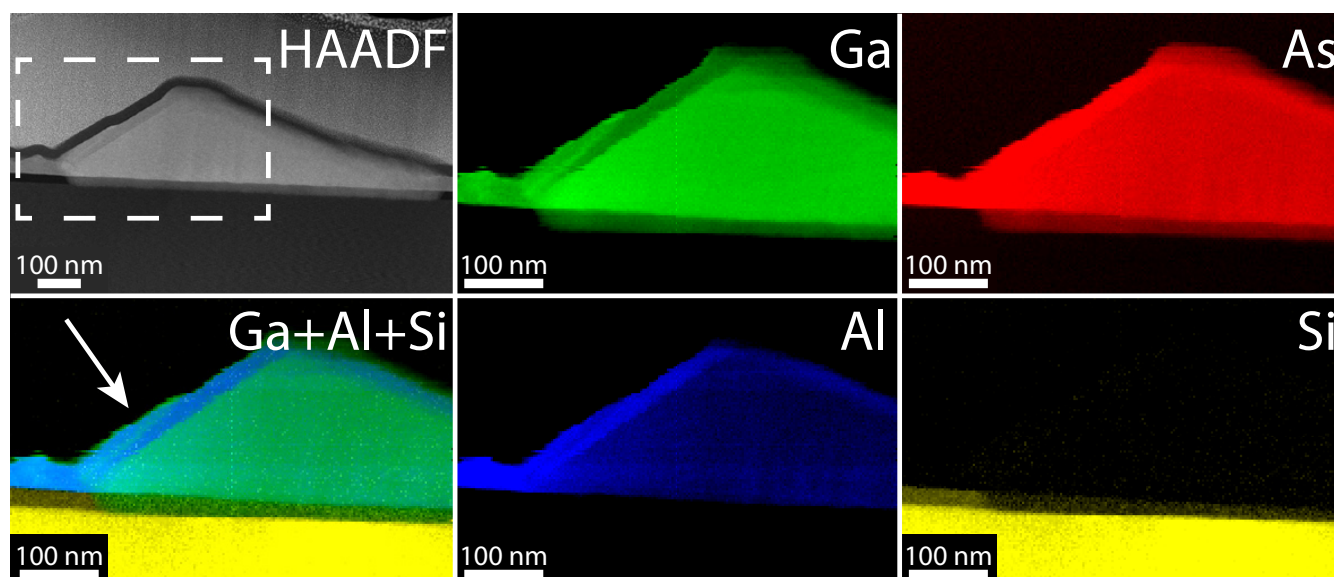


Figure 1 Elemental maps of Ga, As, Al and Si obtained through scanning transmission electron microscopy (STEM) EELS in the indicated area of the high-angle annular dark-field (HAADF) micrograph.

Figure 1 shows elemental composition mapping of main components in nanomembrane (NM). We observe a homogeneous elemental distribution of Ga and As along the NM and no Si diffusion into the membrane. We observe homogeneous distribution of Al in the NM from this view due to the

presence of the $\{110\}$ front and back facets. However, the areal density is not homogeneous at the edges of the membrane, instead getting higher on the short edge.

The AlGaAs shell is covered by a GaAs layer to prevent it from oxidizing. However, we can see that a thin AlGaAs layer is covering the most external GaAs layer in the region close to the intersection between the NM base and its back facet (marked by an arrow in the image). As this layer is formed once the flux of atoms (Ga and As) are closed, it indicates that there might be some diffusion of material from the irregular AlGaAs layer that covers the substrate to the NM itself.

2 HAADF/MAADF images on other defective areas

High-resolution medium-angle annular dark-field (MAADF) and HAADF images of defects are shown in Figure 2.

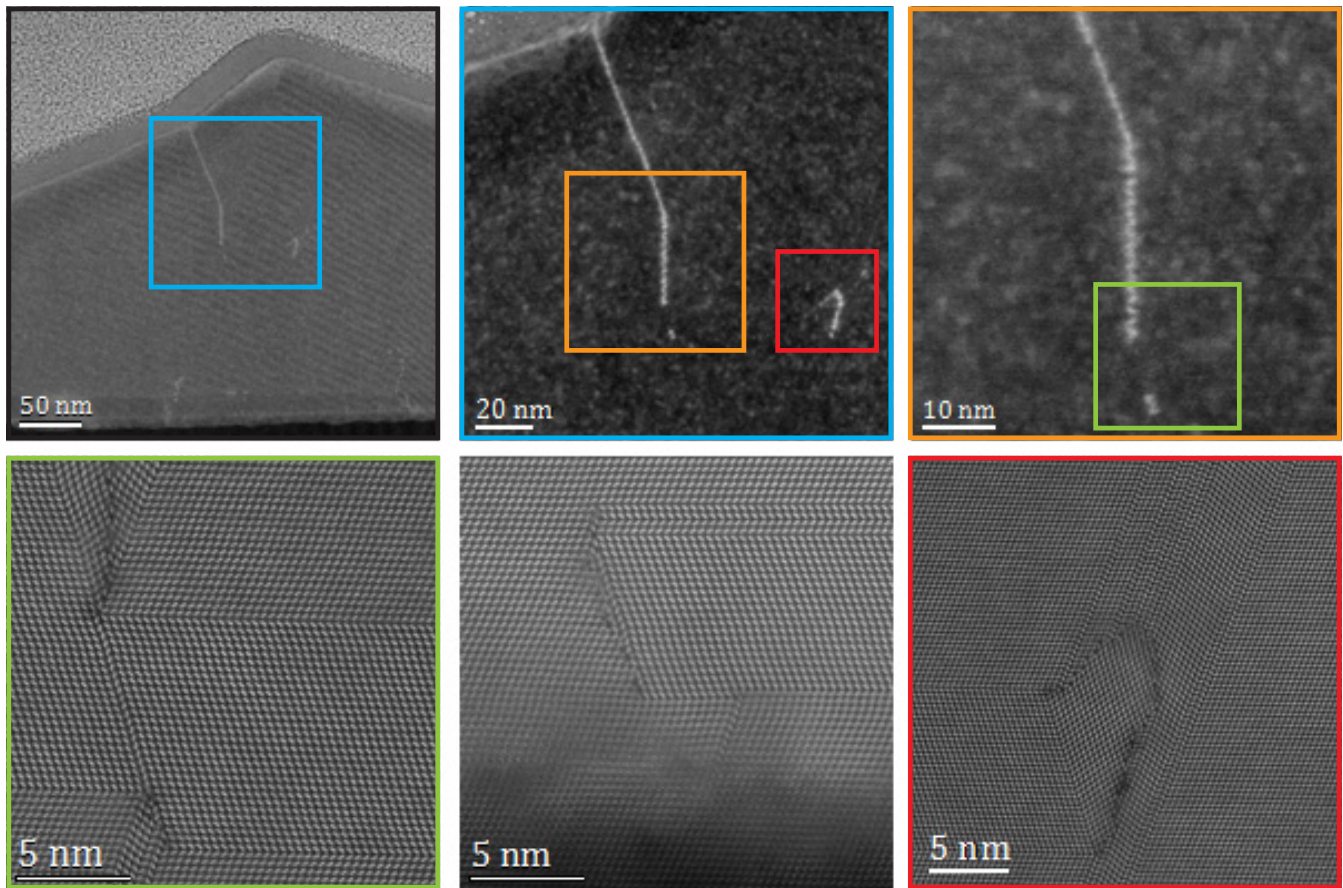


Figure 2 MAADF (top) and HAADF (bottom) micrographs obtained on defective areas of NM B where an accumulation of strain is detected

The accumulation of strain is revealed by the higher intensity shown by these defects in the MAADF images. These defects are formed when twin boundaries in different directions match together.

3 Strain maps

We have performed strain maps from the HAADF high-resolution micrographs. By comparing the measured values of dilatation with the lattice mismatch between Si and relaxed GaAs we can evaluate strain relaxation in the membrane. An example of strain maps at the Si-GaAs interface close to vertices between the NM and the substrate are shown in Figure 3. We observe a compression in GaAs lattice in the first 20 nm, which correspond to the region where the substrate is covered by the SiO₂ mask. Once the material is not constrained by the mask, it gets fully relaxed. Additionally, a slight rotation of the planes is observed (approx. 1.0-1.2° in the region close to the origin of the inclined ($\bar{1}\bar{1}0$) facet of the NM (green square). This phenomenon has been previously observed in other selective-area growth (SAG) one-dimensional (1D) nanostructures.¹

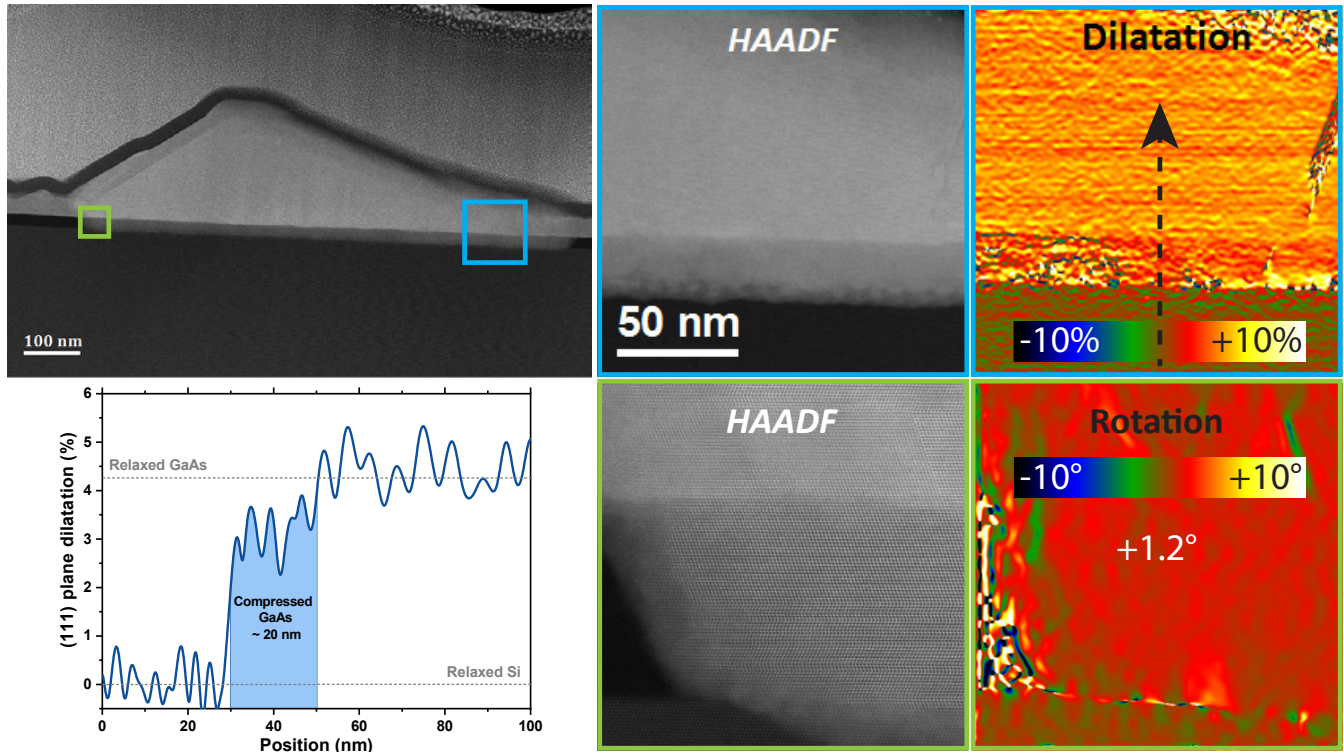


Figure 3 Geometrical phase analysis (GPA) applied to (111) horizontal planes for acquisition of dilatation and rotation of planes maps with Si lattice as reference value. A dilatation profile obtained through the arrow in the dilatation map is shown below.

4 Influence of different pre-growth treatments on the preferential orientation of the NMs

In order to check if we can favour a preferential orientation of the NMs, we tried different treatments of the substrate before NM growth. The additional steps considered include a short predeposition step of Ga or As₄ and the inclusion of an annealing time between the predeposition step and the NM growth. To perform the analysis, we obtained scanning electron microscopy (SEM) images of regions where short NMs were grown (in 80 nm and 170 nm long slits). The preferential alignment is given by the number of NMs whose long axis points towards the $[1\ 1\ \bar{2}]$ direction, divided by the total amount of NMs considered for the analysis. A minimum of 100 NMs per sample were checked for the quantification. The results obtained are summarized in Table 1. As an example, two SEM micrographs of samples 1 and 4 are shown in Figure 4.

We can see that when the substrate is not treated, the NMs are randomly oriented along the $[1\ 1\ \bar{2}]$ or the $[1\ \bar{1}\ \bar{2}]$ directions. However, whenever a pre-treatment of the substrate is applied, the NMs tend to orientate towards the $[1\ 1\ \bar{2}]$ direction. The effect induced on the preferential orientation is enhanced when the duration of the predeposition time is increased or an annealing step is included just before the growth. Good results are obtained either via a Ga or an As₄ exposition of the substrate. By looking at the results, we believe that an improvement of the preferential alignment can be achieved by further increasing the predeposition time.

Sample #	Recipe	Pref. Alignment
1	NM Growth	54%
2	30s Ga Predep + NM Growth	67%
3	60s Ga Predep + NM Growth	77%
4	30s Ga Predep + 5min Anneal + NM Growth	87%
5	3min As Predep + 2min Anneal + NM Growth	88%

Table 1 Preferential alignment sample summary.

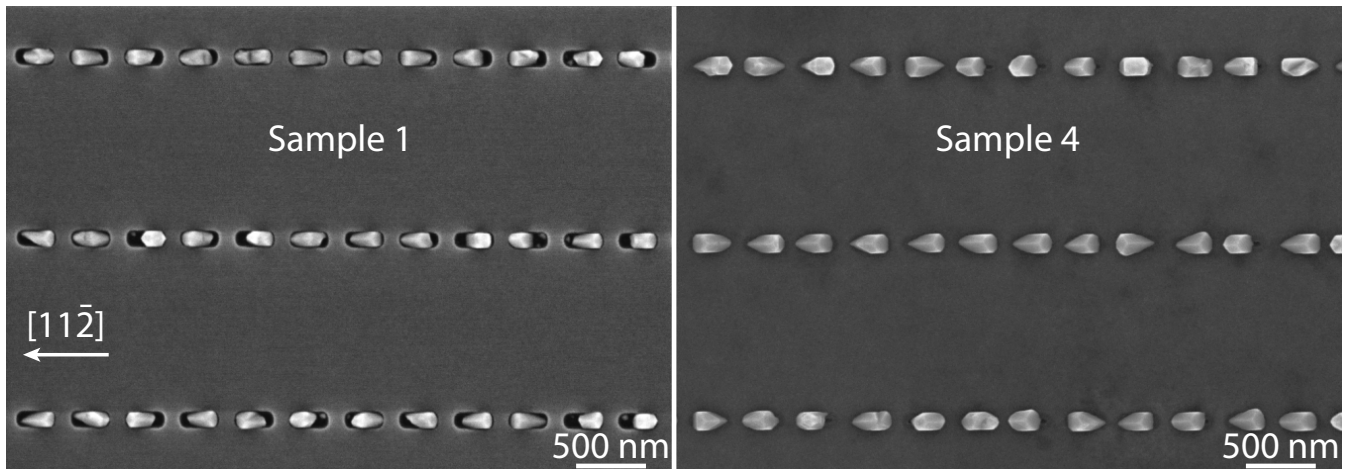


Figure 4 SEM images of Sample 1 (left) and Sample 4 (right), where an improvement of the preferential orientation of the NMs in Sample 4 is evident.

5 Gaussian fit of the PL emission of NM B

Figure 5 shows the photoluminescence (PL) emission of NM B, which was previously represented by the green curve in Figure 3 of the main article. The red curve in Figure 5 corresponds to the experimental spectrum. This spectrum has been fitted by three Gaussian peaks, which are represented in the figure by the blue dotted curves. These three peaks are centred at 826 nm, 836 nm and 851 nm, respectively. The grey line is obtained as the sum of these components. The goodness of the fit is supported by the value of $R^2 = 0.9990$.

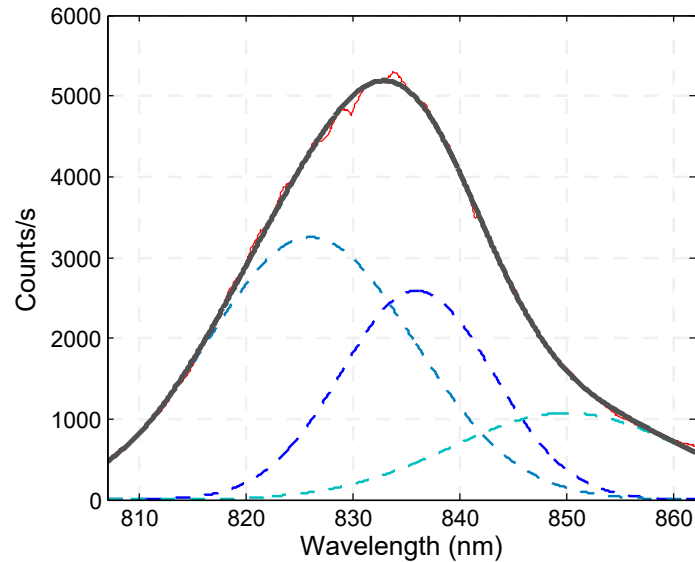


Figure 5 Gaussian fit of the PL emission of NM B (green curve in Figure 3 of the main article).

6 Time-Resolved PL

Time-resolved photoluminescence (TRPL) spectra were acquired for the highest-energy component of each NM. The experimental data has been fitted as the convolution of the instrument response function (IRF) with a double exponential function using an iterative reconvolution algorithm:

$$TRPL(t) = IRF \times (A_1 e^{-t/\tau_1} + A_2 e^{-t/\tau_2})$$

The contribution of each lifetime component is given by its weight, which is calculated using the expression:

$$W_i = 100 \times \frac{A_i \tau_i}{A_1 \tau_1 + A_2 \tau_2}$$

Finally, the effective lifetime is given by:

$$\tau_m = \frac{(A_1 \tau_1 + A_2 \tau_2)}{100}$$

	A_1	τ_1 (ps)	A_2	τ_2 (ps)	W_1 (%)	W_2 (%)	$\langle \tau \rangle$ (ps)
NM A	0.029	1065	0.971	41	43.7	56.3	488
NM B	0.010	726	0.990	30	19	81.0	162

Table 2 TRPL fit results.

The results obtained are shown in Table 2. The contribution of the shorter-lived component to the PL decay is more significant in NM B. This fact, together with the shorter lifetimes detected in NM B, leads to a decrease in the effective lifetime of the charge carriers. The overall effective lifetimes are 488 ps (NM A) and 162 ps (NM B). Previous studies performed on passivated GaAs nanowires (NWs) revealed that the exciton lifetimes can increase from values below 50 ps^{2,3} to values above 1 ns when twins are suppressed.⁴ These values are close to the two time components detected in the analysis of NM A. We thus think that by completely inhibiting the formation of twins in the NMs, the effective lifetimes can be further extended until those measured in defect-free NWs⁴ and in high-quality two-dimensional (2D) GaAs/AlGaAs double heterostructures.⁵

References

- [1] F. Krizek, J. E. Sestoft, P. Aseev, S. Marti-Sanchez, S. Vaitiekėnas, L. Casparis, S. A. Khan, Y. Liu, T. Stankevič, A. M. Whitar, A. Fursina, F. Boekhout, R. Koops, E. Uccelli, L. P. Kouwenhoven, C. M. Marcus, J. Arbiol and P. Krogstrup, *Physical Review Materials*, 2018, **2**, 093401.
- [2] L. V. Titova, T. B. Hoang, H. E. Jackson, L. M. Smith, J. M. Yarrison-Rice, Y. Kim, H. J. Joyce, H. H. Tan and C. Jagadish, *Applied Physics Letters*, 2006, **89**, 173126.
- [3] T. B. Hoang, L. V. Titova, J. M. Yarrison-Rice, H. E. Jackson, A. O. Govorov, Y. Kim, H. J. Joyce, H. H. Tan, C. Jagadish and L. M. Smith, *Nano Letters*, 2007, **7**, 588–595.
- [4] S. Perera, M. A. Fickenscher, H. E. Jackson, L. M. Smith, J. M. Yarrison-Rice, H. J. Joyce, Q. Gao, H. H. Tan, C. Jagadish, X. Zhang and J. Zou, *Applied Physics Letters*, 2008, **93**, 053110.
- [5] D. J. Wolford, G. D. Gilliland, T. F. Kuech, L. M. Smith, J. Martinsen, J. A. Bradley, C. F. Tsang, R. Venkatasubramanian, S. K. Ghandi and H. P. Hjalmarson, *Journal of Vacuum Science and Technology B: Microelectronics and Nanometer Structures*, 1991, **9**, 2369–2376.